GEOLOGY | THE GEOLOGICAL SOCIETY OF AMERICA®

https://doi.org/10.1130/G45501.1

Manuscript received 16 August 2018
Revised manuscript received 18 December 2018
Manuscript accepted 18 December 2018

Published online 18 January 2019

Formation of green rust and elemental sulfur in an analogue for oxygenated ferro-euxinic transition zones of Precambrian oceans

E. Koeksoy[1]*, A. Sundman[1]*, J.M. Byrne[1], R. Lohmayer[2], B. Planer-Friedrich[2], I. Halevy[3], K.O. Konhauser[4], and A. Kappler[1,5]†

[1]Geomicrobiology, University of Tuebingen, 72076 Tuebingen, Germany
[2]Environmental Geochemistry, Bayreuth Center for Ecology and Environmental Research (BayCEER), University of Bayreuth, 95440 Bayreuth, Germany
[3]Department of Earth and Planetary Sciences, Weizmann Institute of Science, Rehovot 76100, Israel
[4]Department of Earth and Atmospheric Sciences, University of Alberta, Edmonton, Alberta T6G 2E3, Canada
[5]Center for Geomicrobiology, Aarhus University, 8000 Aarhus, Denmark

ABSTRACT

For much of the Precambrian era, the bulk ocean was anoxic and Fe(II) rich (ferruginous), except for the first development of shallow ocean oxygenation and temporally/spatially restricted sulfide-rich waters (euxinia) along productive continental margins in the late Archean, which prevailed throughout much of the remaining Precambrian. There is little detail pertaining to transition zones between ferruginous, euxinic, and oxic seawater over the continental shelf that may have played an important role in shaping the composition of the underlying sediment. Here we present spectroscopic data on the Fe and sulfur mineralogy in the Arvadi Spring (Switzerland), a proposed analogue for such conditions. Our study reveals green rust, ferrihydrite, and lepidocrocite as the main Fe minerals. Because the reactivity of green rust differs from that of ferric hydroxides and Fe(II) sulfides, it is important to understand its role in the transfer of metals and nutrients from seawater to underlying sediments, if those sediments are to be used as chemical archives of paleo-seawater. We observed elemental sulfur (S^0) as the dominant sulfur precipitate and found indications for its role in pyrite formation, implying that S^0 could have had a similar role in Precambrian deposition of pyrite-poor or pyrite-rich sediments.

INTRODUCTION

The end of abundant banded iron formation (BIF) deposition (Bekker et al., 2014), and an accompanying increase in black shale deposition by ca. 1.8 Ga (Poulton et al., 2004a), reflects a major transition in seawater composition in the wake of atmospheric oxygenation across the Archean-Proterozoic boundary (Bekker and Holland, 2012). Specifically, shallow seawater became slightly oxygenated (Hardisty et al., 2014), and increased oxidative weathering of continental pyrite (Konhauser et al., 2011) delivered substantial amounts of sulfate to the ocean. The resulting enhancement of sulfate reduction rates in the highly productive regions of upwelling deep water is thought to have resulted in regional growth of the oceanic sulfide pool, where Fe(II) was removed mostly in the form of Fe(II) sulfides (Canfield, 1998).

Although transition zones between ferruginous-euxinic, oxic-euxinic, and oxic-ferruginous water masses likely were a prominent feature in shallow Precambrian oceans, their areal extent, their biogeochemical composition, and the identity and composition of minerals and chemical sediments precipitating from such seawater remain unknown. The analysis of modern habitats that resemble ancient ocean settings, such as Lake Matano (Indonesia; Crowe et al., 2008), Lake Pavin (France; Busigny et al., 2014), Lake Cadagno (Switzerland; Canfield et al., 2010), and Lake La Cruz (Spain; Walter et al., 2014), is an emerging alternative approach to reconstruct paleo-seawater composition and the identity of mineral phases (Koeksoy et al., 2016). For instance, Zegeye et al. (2012) demonstrated that green rust formed in Lake Matano, suggesting a particular role for this mixed-valence Fe mineral as a BIF precursor.

Here we present spectroscopic data of Fe- and S-rich precipitates that formed by biogeochemical processes in a Fe- and S-rich proposed modern analogue for oxygenated ferro-euxinic transition zones of Precambrian oceans, i.e., the Arvadi Spring (Switzerland, 46°40′17.4″N, 9°39′18.8″E; Koeksoy et al., 2018). Our results constrain (1) the identity of Fe and S phases that may have precipitated in oxygenated ferro-euxinic transition zones of the Precambrian ocean, and (2) the possible consequences for nutrient and trace metal bioavailability due to interaction with these phases.

MATERIALS AND METHODS

All samples were collected at the Arvadi Spring (Koeksoy et al., 2018, Fig. DR1 in the GSA Data Repository[1]) and transported on ice and in the dark to the Geomicrobiology laboratory, University of Tuebingen, Germany, for analysis. Water pH, temperature, oxygen saturation, and electrical conductivity were measured in situ (field multimeter, WTW Multi 3430). The Fe(II)/Fe(III) ratio was quantified with the ferrozine

*These authors contributed equally to this work.
†E-mail: andreas.kappler@uni-tuebingen.de

[1]GSA Data Repository item 2019076, expanded sampling details and methods, is available online at http://www.geosociety.org/datarepository/2019/, or on request from editing@geosociety.org.

CITATION: Koeksoy, E., et al, 2019, Formation of green rust and elemental sulfur in an analogue for oxygenated ferro-euxinic transition zones of Precambrian oceans: Geology, v. 47, p. 211–214, https://doi.org/10.1130/G45501.1.

assay (Stookey, 1970) in water samples fixed with 0.5 M HCl. Sulfide was quantified with the methylene blue assay (Cline, 1969) in water samples fixed with 2% (w/v) zinc acetate. Water samples for anion, cation, and dissolved organic carbon (DOC) quantification were filtered (0.45 µm) prior to analyses by ion chromatography (Dionex DX-120, equipped with AS9HC column and AG9HC precolumn) and a carbon analyzer (Elementar High TOC II). Mineral precipitates ("red flocs" and "white flocs") were found as loose aggregates, with red flocs covering the entire spring sediment, and white flocs, which apparently had a lower density, accumulating in a heterogeneous distribution on top of red flocs. Red and white flocs were collected from the sediment top layer in airtight bottles flushed with N_2 gas, transported on ice, and freeze dried in the laboratory. Samples were stored anoxically in the dark at room temperature until analysis.

Synchrotron-based X-ray absorption spectra were collected for red and white floc samples at the Fe and sulfur (S) K-edges at the SUL-X beamline at ANKA, Karlsruhe Institute of Technology (KIT), Germany, and subsequently energy calibrated and averaged using SixPack software (Webb, 2002). Fe spectra were subjected to linear combination fitting (LCF) using Athena software (Ravel and Newville, 2005) and shell-by-shell fitting in Viper software (Klementev, 2001). Additionally, red floc Fe mineralogy was determined with ^{57}Fe Mössbauer spectroscopy at 77 K and subsequent spectra fitting using Recoil software, Voigt-based fitting routine (Lagarec and Rancourt, 1998). White flocs were further subjected to sulfide (Cline, 1969) and elemental S (S^0; Wan et al., 2014) quantification in the Geomicrobiology Laboratory, University of Tuebingen, Germany, and to polysulfide quantification (Rizkov et al., 2004; Kamyshny et al., 2006) in the Environmental Geochemistry Laboratory, University of Bayreuth, Germany.

The water saturation index (SI) with respect to FeS was calculated according to the following, with a solubility product, K_{sp}, of $10^{-5.7}$ for FeS (Rickard, 2006) and {FeS} of unity, considering FeS to be a pure solid phase:

$$SI = \log\left(\frac{IAP}{K_{sp}}\right), \quad (1)$$

where the ion activity product (IAP) is

$$IAP = \frac{\{A\}\{B\}}{\{AB\}} = \frac{\{Fe^{2+}\}\{HS^-\}}{\{FeS\}\{H^+\}}. \quad (2)$$

RESULTS AND DISCUSSION

Water Geochemistry

The water had a pH of 7.8 and a temperature of 7.5 °C, and contained dissolved O_2 at 11.01 mg l^{-1}. Dissolved Fe(II) and sulfide were quantified at 15.6 ± 2.3 µM (n = 3) and 1.8 ± 0.1 µM (n = 4), respectively; no dissolved Fe(III) was detected. Sulfate (8.4 ± 0.0 mM, n = 3), bicarbonate (4.5 ± 0.0 mM, n = 3), magnesium (3.3 ± 0.0 mM, n = 3), and calcium (7.0 ± 0.4 mM, n = 3) constituted the dominating anions and cations. Dissolved organic carbon was detected at 1.16 ± 0.03 mg l^{-1} (n = 3).

The Arvadi Spring water geochemistry is unique in that it contains measureable sulfide and Fe(II) concentrations while being exposed to relatively high levels of oxygen, demonstrating that the system is thermodynamically out of equilibrium and the observed processes are governed by kinetics. S-isotope data (Strauss et al., 2016) and 16S rRNA gene sequencing data of Arvadi Spring sediment (Koeksoy et al., 2018) indicate sulfate reduction as the source of sulfide in the Arvadi water, while dissimilatory Fe(III) reduction is the major source for Fe(II) (Koeksoy et al., 2018). We could not observe a redox gradient within the fully oxygenated pond water due to its shallow depth (~20 cm), and assume anoxic conditions, which would allow anaerobic Fe(III) and sulfate reduction to occur below the first few millimeters of the sediment, similar to the oxygen penetration depth in organic-rich marine sediments (Revsbech et al., 1980).

Iron Mineralogy in Red Flocs

Linear combination fitting (LCF; Fig. 1; Table DR1) and shell-by-shell extended X-ray-absorption fine structure (EXAFS) data fitting of red floc samples (n = 3; Fig. 2; Table DR2) revealed a heterogeneous Fe mineralogy, even within bulk spectra. The EXAFS data fitting corresponded to first-shell oxygen neighbors and second-shell Fe neighbors at distances typical for ferrihydrite and goethite, i.e., ~3.0 and 3.4 Å, respectively (Table DR2). According to the LCF, the Fe(II)-Fe(III) mixed-valence mineral green rust ($[Fe(II)_{1-x}Fe(III)_x(OH)_2]^{x+} \cdot [(x/n)\,A^{n-} \cdot mH_2O]^{x-}$, where x denotes the number of Fe(III) atoms and respective ion charges, A denotes either Cl, SO_4, or CO_3, n denotes the respective ion charge number, and m denotes the number of water molecules) together with the Fe(III) oxyhydroxides lepidocrocite and ferrihydrite are the dominating Fe mineral species in red flocs, with minor contributions from goethite, magnetite, and organically complexed Fe (Fig. 1). Differences between EXAFS and X-ray absorption near edge structure (XANES) LCFs were likely caused by different region sensitivities, with the EXAFS region being more sensitive to the distance, number, and identity of the close neighbor, whereas the XANES region is more sensitive to the oxidation state and coordination environment. Furthermore, the LCFs are associated with uncertainties of 5%–10%. Carbonate as A^{n-} was the dominant anion in the green rust phases. The LCF showed almost no Fe(II) sulfides despite a supersaturation of FeS at a calculated SI of 2.90. It is likely that most Fe(II) sulfides form in the spring sediment, where Fe(II) and sulfide are present at higher concentrations, allowing them to overcome kinetic barriers to nucleation and growth.

Mössbauer spectroscopy data on the red flocs were fitted with a wide paramagnetic doublet (δ [chemical shift] = 1.27 mm/s, ΔE_Q [quadrupole

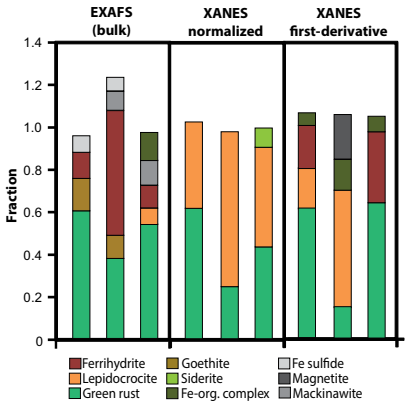

Figure 1. Results of Fe K-edge linear combination fitting of extended X-ray-absorption fine structure (EXAFS) and X-ray absorption near edge structure (XANES) regions in bulk spectra of red floc mineral precipitates from Arvadi Spring (Switzerland). org.—organic.

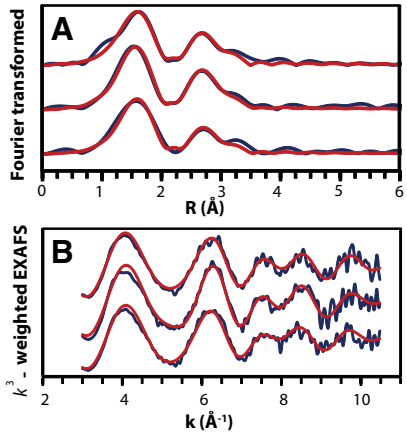

Figure 2. Fourier-transformed (A) and k^3-weighted (B) Fe K-edge extended X-ray-absorption fine structure (EXAFS) for Fe-rich flocs from Arvadi Spring (Switzerland). Blue lines represent experimental data, and red lines fit results from shell-by-shell fitting. k—photo-electron wavenumber; R—bond distance.

splitting] = 2.74 mm/s) that is characteristic of an Fe(II) mineral phase and accounts for 55.6% of the total spectral area (Table DR3; Fig. DR2 in the Data Repository). The parameters of this doublet were consistent with Fe(II) present in green rust (Génin et al., 1998), providing additional support to the LCF data fitting. Due to masking by Fe(III) (oxyhydr) oxides present in the samples, it is difficult to ascertain whether or not the corresponding Fe(III) doublet of green rust, which is necessary for its conclusive identification, is present in the spectra. Nevertheless, the presence of green rust as determined by Mössbauer analysis is in agreement with LCF, in which green rust was also identified.

Green rust precipitation is usually observed during partial Fe(II) oxidation (microbial or abiotic) under mildly alkaline conditions, or upon partial reduction of Fe(III) oxyhydroxides (Usman et al., 2012; Pantke et al., 2012). We suggest both pathways to be possible sources for the Arvadi Spring green rust, as Koeksoy et al. (2018) showed red flocs to be colonized by Fe(II)-oxidizing and Fe(III)-reducing microorganisms. In either case, the formation of green rust is controlled by the kinetics of (bio)chemical reactions and mineral precipitation in the Arvadi water and sediments, as it is metastable and not expected to persist in either oxidizing or reducing conditions (Halevy et al., 2017).

Iron and Sulfur Mineralogy in White Flocs

We found white flocs to be dominated by S^0 (~2472 eV) and sulfate (SO_4^{2-}; ~2481 eV) according to the peak fit of the S K-edge bulk spectra (Fig. 3C; Table DR4). S^0 was quantified by high-performance liquid chromatography at 185 ± 41 mg g^{-1} dry flocs (18.5% of the dry weight), while the sulfate peak most likely is the result of $MgSO_4$ or $CaSO_4$ precipitation through the concentration of SO_4^{2-}, Mg^{2+}, and/or Ca^{2+} in residual Arvadi pond water during freeze drying. Polysulfides in the form of S_5^{2-} were detected at much lower concentrations (186 ± 72 µg g^{-1} dry flocs), similar to low concentrations of hydrogen sulfide and other polysulfides in the Arvadi water (at or below detection limits of a few µM for polysulfides, 1 µM for H_2S), indicating their quick turnover to more oxidized S^0 and sulfate.

Aqueous S^0 forms by microbial or abiotic partial sulfide oxidation, and upon reaching supersaturation, solid S^0 precipitates (Garcia and Druschel, 2014). Koeksoy et al. (2018) showed *Thiothrix* spp., aerobic sulfide-oxidizing microorganisms that store solid S^0 in intracellular "sulfur globules" (Nielsen et al., 2000), to dominate the Arvadi Spring microbial community based on 16S rRNA gene sequence abundance. We therefore suggest that microbial sulfide oxidation is a significant S^0 formation mechanism in the Arvadi Spring, while an alternative pathway is microbial (Lohmayer et al., 2014) or abiotic (e.g., Poulton et al., 2004b) Fe(III) reduction coupled to sulfide oxidation. Once S^0 is formed, S^0 oxidation or reduction kinetics under Arvadi Spring conditions are slow enough to allow its persistence in white flocs.

White flocs contained a minor fraction of Fe (0.08 wt% or 837.8 µg g^{-1} dry flocs) with a high mineralogical heterogeneity (Figs. 3A and 3B) that varied depending on the prevailing Fe and S concentrations. For instance, ~50% of the mineral species at hotspots (HP) in the dried samples with high S and low Fe concentrations corresponded to green rust, mackinawite, and pyrite. In contrast, hotspots with high S and Fe concentrations (HP1, HP4, HP6, and HP7) were dominated by ferrihydrite and lepidocrocite (60%–70% of the Fe species) and contained minor green rust, pyrite, mackinawite, and potentially some Fe-organic complexes (Fig. 3). The S mineralogy also varied, with S^0 being dominant under high S concentrations (HP1, HP2, HP4, HP6, and HP7 according to µ-XRF [micro X-ray fluorescence]), whereas more sulfate was detected in samples with low or very low S concentrations (HP3 and HP5; Fig. 3C). Collectively, these results imply that pyrite nucleation in the Arvadi Spring is promoted by high S concentrations that in turn come along with S^0 prevalence, being consistent with previous studies suggesting an important role for S^0 in pyrite nucleation (Rickard and Luther, 2007; Wan et al., 2017).

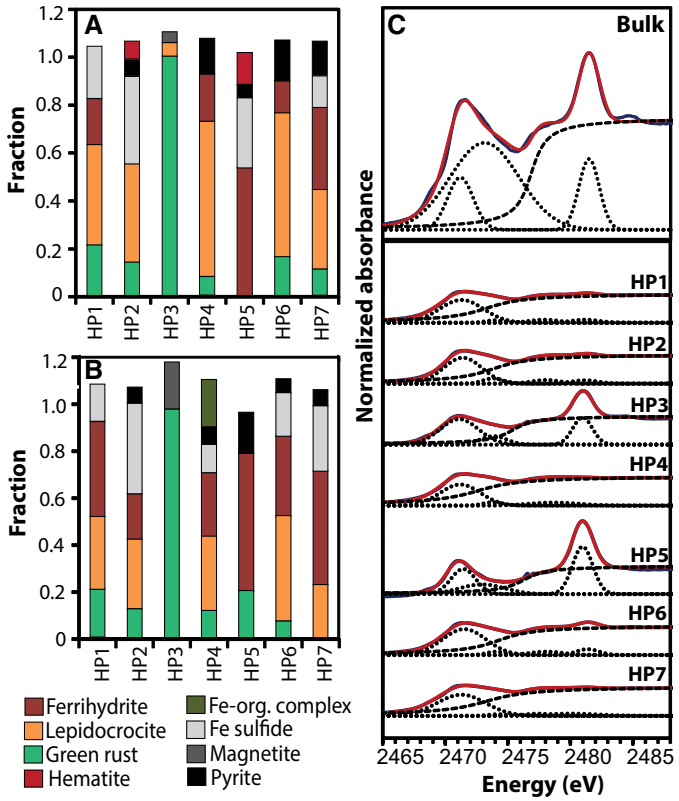

Figure 3. A,B: Linear combination fitting of normalized (A) and first-derivative (B) Fe K-edge µ-XANES (micro X-ray absorption near edge structure) of hotspots HP1–HP7 in white flocs from Arvadi Spring (Switzerland). org.—organic. C: Results of peak fits of S K-edge XANES bulk and hotspot spectra. Black dotted lines correspond to experimental data, red lines to fits, and black dashed lines to individual peak and step functions used in fitting.

Implications for Precambrian Ocean Biogeochemistry

The geochemistry, mineralogy, and microbiology of ferruginous and euxinic waters that encroached on oxygen-bearing surface waters is poorly understood. Koeksoy et al. (2018) proposed the Arvadi Spring as a modern analogue of Precambrian ocean mixing zones between ferruginous and euxinic, oxic and euxinic, or oxic and ferruginous waters, or all three. The Arvadi Spring not only suggests that such water masses may have contained appreciable concentrations of both Fe(II) and sulfide, but also constrains the mineralogy of precipitates from these waters upon exposure to oxygen.

Our data support previous suggestions of ferrihydrite and lepidocrocite as important precursors to crystalline and more stable Fe mineral phases (Posth et al., 2013). Most notably, however, our findings support the recent suggestion of green rust as a highly reactive BIF precursor based on experimental and modeling data (Halevy et al., 2017), and show that green rust can form not only in modern analogues for ferruginous oceans (Zegeye et al., 2012) but also in model habitats for oxygenated ferro-euxinic transition zones. Green rust formation would have had important implications for nutrient and trace metal cycling, considering strong sorption of nickel (Zegeye et al., 2012), phosphate (Hansen and Poulsen, 1999), and silica (Kwon et al., 2007) to green rust, as well as immobilization of trace metals such as uranium (O'Loughlin et al., 2003) and chromium (Williams and Scherer, 2001).

Our study further highlights an important role for S^0 in oxygenated ferro-euxinic mixing waters. Similar to green rust, S^0 is metastable and was not preserved in the rock record, but both are expected to transform into more stable phases during diagenesis. Briefly, we expect green rust to transform into more stable Fe mineral phases (Fig. DR3), while S^0 would react with pore-water sulfide to form dissolved or surface-associated

polysulfides, which rapidly react with FeS precursors to pyrite or participates in organic matter sulfurization. Further laboratory and modeling experiments are required to confirm the ubiquity of green rust and S^0 in oxygenated ferro-euxinic environments.

ACKNOWLEDGMENTS

This work was supported by the German Research Foundation (DFG) grant KA 1736/27-1. We thank Joerg Goettlicher and Ralph Steininger from the KIT ANKA facilities, and Cindy Lockwood for assistance during the data collection process. We also thank Nicolas Mayot for providing the Arvadi Spring location map. The spectra of the Fe model compounds were provided by Thomas Borch (Colorado State University, USA). We thank Simon Poulton and three anonymous reviewers for helpful suggestions.

REFERENCES CITED

Bekker, A., and Holland, H.D., 2012, Oxygen overshoot and recovery during the early Paleoproterozoic: Earth and Planetary Science Letters, v. 317–318, p. 295–304, https://doi.org/10.1016/j.epsl.2011.12.012.

Bekker, A., Planavsky, N.J., Krapež, B., Rasmussen, B., Hofmann, A., Slack, J.F., Rouxel, O.J., and Konhauser, K.O., 2014, Iron formations: Their origins and implications for ancient seawater chemistry, *in* Mackenzie, F.T., ed., Treatise on Geochemistry (second edition), Volume 9: Sediments, Diagenesis and Sedimentary Rocks: Waltham, Massachusetts, Elsevier, p. 561–628, https://doi.org/10.1016/B978-0-08-095975-7.00719-1.

Busigny, V., Planavsky, N.J., Jézéquel, D., Crowe, S., Louvat, P., Moureau, J., Viollier, E., and Lyons, T.W., 2014, Iron isotopes in an Archean ocean analogue: Geochimica et Cosmochimica Acta, v. 133, p. 443–462, https://doi.org/10.1016/j.gca.2014.03.004.

Canfield, D.E., 1998, A new model for Proterozoic ocean chemistry: Nature, v. 396, p. 450–453, https://doi.org/10.1038/24839.

Canfield, D.E., Farquhar, J., and Zerkle, A.L., 2010, High isotope fractionations during sulfate reduction in a low-sulfate euxinic ocean analog: Geology, v. 38, p. 415–418, https://doi.org/10.1130/G30723.1.

Cline, J.D., 1969, Spectrophotometric determination of hydrogen sulfide in natural waters: Limnology and Oceanography, v. 14, p. 454–458, https://doi.org/10.4319/lo.1969.14.3.0454.

Crowe, S.A., Jones, C., Katsev, S., Magen, C., O'Neill, A.H., Sturm, A., Canfield, D.E., Haffner, G.D., Mucci, A., and Sundby, B., 2008, Photoferrotrophs thrive in an Archean Ocean analogue: Proceedings of the National Academy of Sciences of the United States of America, v. 105, p. 15,938–15,943, https://doi.org/10.1073/pnas.0805313105.

Garcia, A.A., Jr., and Druschel, G.K., 2014, Elemental sulfur coarsening kinetics: Geochemical Transactions, v. 15, 11, https://doi.org/10.1186/s12932-014-0011-z.

Génin, J.-M.R., Bourrié, G., Trolard, F., Abdelmoula, M., Jaffrezic, A., Refait, P., Maitre, V., Humbert, B., and Herbillon, A., 1998, Thermodynamic equilibria in aqueous suspensions of synthetic and natural Fe(II)–Fe(III) green rusts: Occurrences of the mineral in hydromorphic soils: Environmental Science & Technology, v. 32, p. 1058–1068, https://doi.org/10.1021/es970547m.

Halevy, I., Alesker, M., Schuster, E.M., Popovitz-Biro, R., and Feldman, Y., 2017, A key role for green rust in the Precambrian oceans and the genesis of iron formations: Nature Geoscience, v. 10, p. 135–139, https://doi.org/10.1038/ngeo2878.

Hansen, H.C.B., and Poulsen, I.F., 1999, Interaction of synthetic sulphate "green rust" with phosphate and the crystallization of vivianite: Clays and Clay Minerals, v. 47, p. 312–318, https://doi.org/10.1346/CCMN.1999.0470307.

Hardisty, D.S., Lu, Z., Planavsky, N.J., Bekker, A., Philippot, P., Zhou, X., and Lyons, T.W., 2014, An iodine record of Paleoproterozoic surface ocean oxygenation: Geology, v. 42, p. 619–622, https://doi.org/10.1130/G35439.1.

Kamyshny, A., Ekeltchik, I., Gun, J., and Lev, O., 2006, Method for the determination of inorganic polysulfide distribution in aquatic systems: Analytical Chemistry, v. 78, p. 2631–2639, https://doi.org/10.1021/ac051854a.

Klementev, K.V., 2001, *VIPER* freeware: Journal of Physics D: Applied Physics, v. 34, p. 209–217, https://doi.org/10.1088/0022-3727/34/2/309.

Koeksoy, E., Halama, M., Konhauser, K.O., and Kappler, A., 2016, Using modern ferruginous habitats to interpret Precambrian banded iron formation deposition: International Journal of Astrobiology, v. 15, p. 205–217, https://doi.org/10.1017/S1473550415000373.

Koeksoy, E., et al., 2018, A case study for late Archean and Proterozoic biogeochemical iron- and sulphur cycling in a modern habitat—The Arvadi Spring: Geobiology, v. 16, p. 353–368, https://doi.org/10.1111/gbi.12293.

Konhauser, K.O., et al., 2011, Aerobic bacterial pyrite oxidation and acid drainage during the Great Oxidation Event: Nature, v. 478, p. 369–373, https://doi.org/10.1038/nature10511.

Kwon, S.K., Kimijima, K., Kanie, K., Suzuki, S., Muramatsu, A., Saito, M., Shinoda, K., and Waseda, Y., 2007, Influence of silicate ions on the formation of goethite from green rust in aqueous solution: Corrosion Science, v. 49, p. 2946–2961, https://doi.org/10.1016/j.corsci.2007.01.007.

Lagarec, K., and Rancourt, D.G., 1998, Recoil-Mössbauer spectral analysis software for Windows: Ottawa, University of Ottawa, 40 p.

Lohmayer, R., Kappler, A., Lösekann-Behrens, T., and Planer-Friedrich, B., 2014, Sulfur species as redox partners and electron shuttles for ferrihydrite reduction by *Sulfurospirillum deleyianum*: Applied and Environmental Microbiology, v. 80, p. 3141–3149, https://doi.org/10.1128/AEM.04220-13.

Nielsen, P.H., De Muro, M.A., and Nielsen, J.L., 2000, Studies on the in situ physiology of *Thiothrix* spp. present in activated sludge: Environmental Microbiology, v. 2, p. 389–398, https://doi.org/10.1046/j.1462-2920.2000.00120.x.

O'Loughlin, E.J., Kelly, S.D., Cook, R.E., Csencsits, R., and Kemner, K.M., 2003, Reduction of uranium(VI) by mixed iron(II)/iron(III) hydroxide (green rust): Formation of UO_2 nanoparticles: Environmental Science & Technology, v. 37, p. 721–727, https://doi.org/10.1021/es0208409.

Pantke, C., Obst, M., Benzerara, K., Morin, G., Ona-Nguema, G., Dippon, U., and Kappler, A., 2012, Green rust formation during Fe(II) oxidation by the nitrate-reducing *Acidovorax* sp. strain BoFeN1: Environmental Science & Technology, v. 46, p. 1439–1446, https://doi.org/10.1021/es2016457.

Posth, N.R., et al., 2013, Simulating Precambrian banded iron formation diagenesis: Chemical Geology, v. 362, p. 66–73, https://doi.org/10.1016/j.chemgeo.2013.05.031.

Poulton, S.W., Fralick, P.W., and Canfield, D.E., 2004a, The transition to a sulphidic ocean ~1.84 billion years ago: Nature, v. 431, p. 173–177, https://doi.org/10.1038/nature02912.

Poulton, S.W., Krom, M.D., and Raiswell, R., 2004b, A revised scheme for the reactivity of iron (oxyhydr)oxide minerals towards dissolved sulfide: Geochimica et Cosmochimica Acta, v. 68, p. 3703–3715, https://doi.org/10.1016/j.gca.2004.03.012.

Ravel, B., and Newville, M., 2005, ATHENA, ARTEMIS, HEPHAESTUS: Data analysis for X-ray absorption spectroscopy using IFEFFIT: Journal of Synchrotron Radiation, v. 12, p. 537–541, https://doi.org/10.1107/S0909049505012719.

Revsbech, N.P., Sorensen, J., Blackburn, T.H., and Lomholt, J.P., 1980, Distribution of oxygen in marine sediments measured with microelectrodes: Limnology and Oceanography, v. 25, p. 403–411, https://doi.org/10.4319/lo.1980.25.3.0403.

Rickard, D., 2006, The solubility of FeS: Geochimica et Cosmochimica Acta, v. 70, p. 5779–5789, https://doi.org/10.1016/j.gca.2006.02.029.

Rickard, D., and Luther, G.W., 2007, Chemistry of iron sulfides: Chemical Reviews, v. 107, p. 514–562, https://doi.org/10.1021/cr0503658.

Rizkov, D., Lev, O., Gun, J., Anisimov, B., and Kuselman, I., 2004, Development of in-house reference materials for determination of inorganic polysulfides in water: Accreditation and Quality Assurance, v. 9, p. 399–403, https://doi.org/10.1007/s00769-004-0788-z.

Stookey, L.L., 1970, Ferrozine—A new spectrophotometric reagent for iron: Analytical Chemistry, v. 42, p. 779–781, https://doi.org/10.1021/ac60289a016.

Strauss, H., Chmiel, H., Christ, A., Fugmann, A., Hanselmann, K., Kappler, A., Königer, P., Lutter, A., Siedenberg, K., and Teichert, B.M.A., 2016, Multiple sulphur and oxygen isotopes reveal microbial sulphur cycling in spring waters in the Lower Engadin, Switzerland: Isotopes in Environmental and Health Studies, v. 52, p. 75–93, https://doi.org/10.1080/10256016.2015.1032961.

Usman, M., Hanna, K., Abdelmoula, M., Zegeye, A., Faure, P., and Ruby, C., 2012, Formation of green rust via mineralogical transformation of ferric oxides (ferrihydrite, goethite and hematite): Applied Clay Science, v. 64, p. 38–43, https://doi.org/10.1016/j.clay.2011.10.008.

Walter, X.A., Picazo, A., Miracle, M.R., Vicente, E., Camacho, A., Aragno, M., and Zopfi, J., 2014, Phototrophic Fe(II)-oxidation in the chemocline of a ferruginous meromictic lake: Frontiers in Microbiology, v. 5, p. 713, https://doi.org/10.3389/fmicb.2014.00713.

Wan, M., Shchukarev, A., Lohmayer, R., Planer-Friedrich, B., and Peiffer, S., 2014, Occurrence of surface polysulfides during the interaction between ferric (hydr)oxides and aqueous sulfide: Environmental Science & Technology, v. 48, p. 5076–5084, https://doi.org/10.1021/es405612f.

Wan, M., Schroder, C., and Peiffer, S., 2017, Fe(III):S(-II) concentration ratio controls the pathway and the kinetics of pyrite formation during sulfidation of ferric hydroxides: Geochimica et Cosmochimica Acta, v. 217, p. 334–348, https://doi.org/10.1016/j.gca.2017.08.036.

Webb, S.M., 2002, Sam's interface for XAS package (SixPACK): Menlo Park, California, https://www-ssrl.slac.stanford.edu/xraywiki/xraywiki.php?n=BeamLine02.SIXPACK.

Williams, A.G.B., and Scherer, M.M., 2001, Kinetics of Cr(VI) reduction by carbonate green rust: Environmental Science & Technology, v. 35, p. 3488–3494, https://doi.org/10.1021/es010579g.

Zegeye, A., et al., 2012, Green rust formation controls nutrient availability in a ferruginous water column: Geology, v. 40, p. 599–602, https://doi.org/10.1130/G32959.1.

Printed in USA